American Mineralogist, Volume 90, pages 262–265, 2005

LETTER

Stability and equation of state of $MgGeO_3$ post-perovskite phase

KEI HIROSE,[1,*] KATSUYUKI KAWAMURA,[1] YASUO OHISHI,[2] SHIGEHIKO TATENO,[1] AND NAGAYOSHI SATA[3]

[1]Department of Earth and Planetary Sciences, Tokyo Institute of Technology, Ookayama, Meguro, Tokyo 152-8551, Japan
[2]Japan Synchrotron Radiation Research Institute, Mikazuki-cho, Sayo-gun, Hyogo 679-5198, Japan
[3]Institute for Research on Earth Evolution, Japan Agency for Marine-Earth Science and Technology, Natsushima-cho, Yokosuka, Kanagawa 237-0061, Japan

ABSTRACT

A phase transition of $MgGeO_3$ perovskite was examined at high-pressure and -temperature using synchrotron X-ray diffraction measurements. The results demonstrate that it transforms to a $CaIrO_3$-type post-perovskite phase above 63 GPa at 1800 K. The density increase is 1.5% at the transition pressure. These observations confirm that $MgGeO_3$ is a low-pressure analogue to $MgSiO_3$, for which a similar phase transition was recently found above 125 GPa and 2500 K. The unit-cell parameters of $MgGeO_3$ post-perovskite phase obtained at 300 K during decompression from 79 to 6 GPa show that the **b**-axis is significantly more compressible than are the **a**- and **c**-axes, which could be due to the GeO_6-octahedral sheet stacking structure along **b**. The bulk modulus was determined to be K_0 = 192(±5) GPa with a fixed pressure derivative of the bulk modulus, K', of 4.

INTRODUCTION

Recently Murakami et al. (2004) discovered a novel phase transition from perovskite to post-perovskite phase with a $CaIrO_3$-type structure in $MgSiO_3$ above 125 GPa and 2500 K, corresponding to the lowermost mantle conditions. The stability and phase transitions of $MgSiO_3$ perovskite, however, have long been controversial (e.g., Saxena et al. 1996; Shim et al. 2001). It is known that germanates act as low-pressure analogues to silicates due to the larger size of the Ge cation and $MgGeO_3$ exhibits the same phase transition sequence as $MgSiO_3$ with increasing pressure (Ozima and Akimoto 1983; Ross and Navrotsky 1988; Leinenweber et al. 1994). It is therefore expected that, similarly to $MgSiO_3$ perovskite, $MgGeO_3$ perovskite transforms to the $CaIrO_3$-type post-perovskite phase. Previous experimental studies showed that $MgGeO_3$ perovskite with a $GdFeO_3$-type structure is stable above 23 GPa (Ito and Matsui 1979; Leinenweber et al. 1994). Here we examined the stable phases in $MgGeO_3$ over a wide pressure range at high temperatures, from 39 GPa and 1850 K to 103 GPa and 2030 K, using a combination of laser-heated diamond-anvil cell (LHDAC) techniques and synchrotron X-ray diffraction measurements.

The $MgSiO_3$ post-perovskite phase may be a dominant mineral in the D'' layer, and therefore its elastic properties are of importance in the interpretation of seismic observations. Murakami et al. (2004) showed that the $MgSiO_3$ post-perovskite phase exhibits a strong single-crystal elastic anisotropy on the basis of molecular dynamics (MD) calculations. Here we present a new experimental evidence for the compression behavior of the post-perovskite phase using $MgGeO_3$ as an analogue material.

EXPERIMENTAL PROCEDURES

High-pressure and high-temperature conditions were generated using LHDAC techniques. The starting material was a commercially available $MgGeO_3$ orthoenstatite powder. It was mixed with platinum black that served both as an internal pressure standard and a laser absorber. The sample mixture was embedded between layers of pure $MgGeO_3$ powder unmixed with platinum. They were compressed with a rhenium gasket and 300 μm culet diamond anvils. We heated the sample from both sides with a focused multimode continuous wave Nd:YAG laser. The temperature was measured from one side by the spectroradiometric method (Watanuki et al. 2001).

Angle-dispersive X-ray diffraction spectra were collected with an imaging plate at BL10XU of SPring-8. Exposure time was 1 to 3 min. A monochromatic incident X-ray beam with a wavelength of 0.4133 Å was collimated to 20 μm in diameter. The two-dimensional X-ray diffraction image was integrated as a function of 2θ to give a conventional one-dimensional diffraction profile using the fit-2D program (Hammersley 1996).

The uncertainty in temperature within the 20 μm area from which X-ray diffraction data was collected was about ±10% (e.g., Kurashina et al. 2004). Pressure was determined using the equation of state of platinum proposed by Holmes et al. (1989) using the (111), (200), or (220) lines, depending on the peak overlap. The uncertainty in pressure was less than ±0.6 GPa at room temperature and ±1.3 to 2.6 GPa at 1700–2230 K. The greater errors at high temperatures were due to large uncertainties in temperature in the application of the *P-V-T* equation of state. The diffraction patterns were repeatedly collected at high temperatures and at room temperature before and after heating.

RESULTS

We conducted two separate sets of experiments. In the first one, the sample was compressed at room temperature to 39 GPa and subsequently heated for 11 minutes at 39–42 GPa and 1710–1850 K. The diffraction peaks of orthorhombic perovskite phase (space group *Pbnm*) appeared within 2 min and did not change with further heating. We then compressed this sample to 94 GPa at room temperature and reheated it for 41 min at 101–103 GPa and 2030–2230 K. New peaks appeared within 2 min during heating, while peaks from perovskite became weak with time. The pattern collected at room temperature after 41 min heating consist predominantly of these new peaks and platinum with minor perovskite peaks [(002) and (112)] (Fig. 1). We calculated the atomic positions and interatomic distances by the Reitveld analysis using RIETAN-2000 program (Izumi and Ikeda 2000) and MD calculations (Murakami et al. 2004). The

* E-mail: kei@geo.titech.ac.jp

0003-004X/05/0001–262$05.00/DOI:10.2138/am.2005.1702

peak positions and intensities of these new peaks are consistent with those calculated for the $CaIrO_3$-type post-perovskite phase (space group *Cmcm*). The diffraction pattern from the Rietveld refinement with preferred orientation of the sample corresponds best with the observed pattern. The observed and calculated diffraction patterns for the post-perovskite phase are presented in Figure 1 and Table 1. The atomic coordinates and interatomic distances based on the Rietveld analysis and the MD calculations are given in Table 2.

In the second set of experiments, the pressure of the phase transition was precisely determined. Similarly to the first experiment, the perovskite phase was first synthesized by heating to 1700 K for 5 min at 60 GPa. The sample was quenched to room temperature at 52 GPa, and was then further compressed to 60 GPa. With heating to 1820–1960 K at 67–75 GPa, intermittently for a total of 45 min, peaks from the post-perovskite phase were again found in the diffraction patterns, coexisting with those from perovskite. The unit-cell volume of the post-perovskite phase is smaller by 1.5% than that of the coexisting perovskite phase at 61 GPa and 300 K. These observations suggest that such *P-T* conditions are within the stability of the post-perovskite phase but are close to the phase transition boundary. The stabilities of the perovskite and post-perovskite phases are summarized in Figure 2. The phase transition boundary is located at 63 GPa and 1800 K.

The equation of state for the $MgGeO_3$ post-perovskite phase was also determined at room temperature during decompression in the first set of experiments. The press load was decreased stepwise from 79 GPa. The entire sample was heated to 1500–1700 K at each pressure by scanning a laser beam for several minutes to reduce pressure gradient across the sample. Heating was not done at 6 GPa, since part of the sample transformed back to the perovskite phase during heating at 20 GPa. The post-perovskite phase disappeared upon decompression to

TABLE 1. Observed and Rietveld-refined diffraction pattern of $MgGeO_3$ post-perovskite phase at 78 GPa and 300 K

hkl	d_{obs} (Å)	d_{ref} (Å)	Δd (Å)	I_{obs}
020	4.2384	4.2364	0.0020	90
002	3.2212	3.2215	–0.0003	20
022	2.5645	2.5643	0.0002	82
110	2.4967	2.4967	0.0000	90
040	2.1187	2.1182	0.0005	23
041	2.0125	2.0122	0.0003	3
112	1.9744	1.9734	0.0010	27
130	1.9177	1.9179	–0.0002	100
023	1.9177	1.9156	0.0021	
131	1.8383	1.8382	0.0001	34
042	1.7700	1.7699	0.0001	7
132	1.6482	1.6479	0.0003	64
113	1.6286	1.6282	0.0004	8
004	1.6098	1.6107	–0.0009	13
024	1.5048	1.5056	–0.0008	5
133	1.4302	1.4305	–0.0003	2
150	1.4214	1.4217	–0.0003	16
060	1.4120	1.4121	–0.0001	3
151	1.3879	1.3883	–0.0004	5
114	1.3535	1.3535	0.0000	20
200*	–	1.3063	–	–
152	1.3007	1.3007	0.0000	38
062	1.2932	1.2933	–0.0001	28
044	1.2818	1.2821	–0.0003	11
220	1.2479	1.2483	–0.0004	7
134	1.2333	1.2334	–0.0001	9
202	1.2110	1.2106	0.0004	3
222	1.1642	1.1640	0.0002	16

Notes: The refined XRD pattern is based on the orthorhombic unit cell: $a = 2.6127$, $b = 8.4728$, and $c = 6.4429$ Å ($Z = 4$).
* Peak overlapping with platinum.

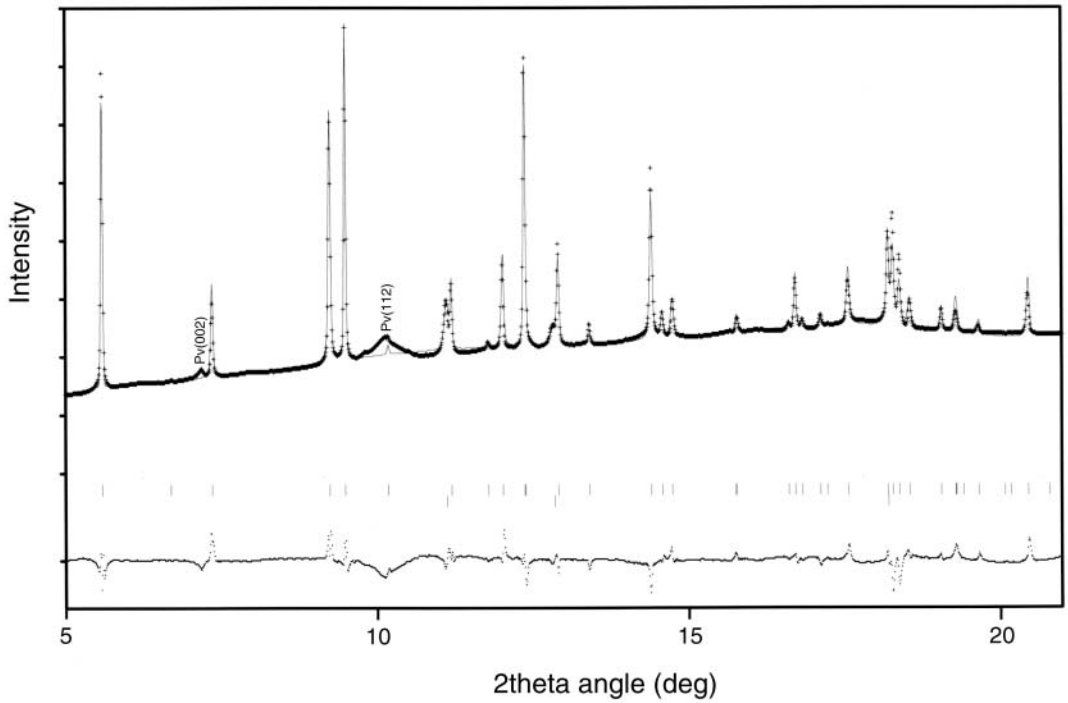

FIGURE 1. Observed and fitted X-ray diffraction pattern of the $MgGeO_3$ post-perovskite phase ($CaIrO_3$-type structure) at 78 GPa and 300 K. Crosses represent the observed data. The difference profile is on the same scale. Vertical bars indicate the calculated positions of the diffraction peaks; top, $CaIrO_3$-type $MgGeO_3$ phase; bottom, platinum. Minor peaks $MgGeO_3$ perovskite (002) and (112) peaks are also included in the observed pattern.

the ambient pressure.

The unit-cell parameters and volumes of the $MgGeO_3$ post-perovskite phase were obtained in a pressure range from 79 to 6 GPa at 300 K (Table 3). The relative cell length along each axis is plotted as a function of pressure in Figure 3. As shown, $MgGeO_3$ post-perovskite phase is elastically anisotropic; the **b**-axis is approximately 30% to 50% more compressible than the **a**- and **c**-axes. To determine the elastic parameters, the *P*-*V* data were fitted to the Birch-Murnaghan equation of state (Birch 1947) (Fig. 4):

$$P = 1.5\ K_0\,(x^{-7} - x^{-5})[1 + 0.75(K_0' - 4)(x^{-2} - 1)]$$

where $x = (V/V_0)^{1/3}$, and V_0, K_0, and K_0' are the volume, isothermal bulk modulus, and its first pressure derivative, respectively, at ambient conditions. The bulk modulus, K_0, was determined to be 210(±20) GPa with $K_0' = 3.5(\pm0.5)$ and $V_0 = 182.2(\pm1.1)$ Å^3. When K_0' was fixed at 4, we obtained $K_0 = 192(\pm5)$ GPa and $V_0 = 183.1(\pm0.8)$ Å^3. This value of K_0 is greater than those for other $MgGeO_3$ polymorphs reported in the previous studies [K_0 = 187(±2) GPa for ilmenite-type phase](Sato et al. 1977; Ashida et al. 1985).

TABLE 2. Atomic coordinates and interatomic distances in $MgGeO_3$ post-perovskite phase at 78 GPa and 300 K

		Rietveld analysis	MD model
Atomic coordinates			
Mg	x	0.0	0.0
	y	0.2547	0.2550
	z	0.25	0.25
Ge	x	0.0	0.0
	y	0.0	0.0
	z	0.0	0.0
O1	x	0.0	0.0
	y	0.9330	0.9220
	z	0.25	0.25
O2	x	0.0	0.0
	y	0.6256	0.6280
	z	0.4383	0.4375
Interatomic distances (Å)			
Mg-O1		1.995 (x2)	1.924 (x2)
Mg-O2		2.090 (x4)	2.077 (x4)
		2.247 (x2)	2.242 (x2)
Mg-Mg		2.612	2.612
Mg-Ge		2.689 (x2)	2.691 (x2)
Ge-O1		1.706 (x2)	1.739 (x2)
Ge-O2		1.730 (x4)	1.743 (x4)
O1-O2		2.414 (x4)	2.435 (x4)
		2.444 (x4)	2.490 (x4)
O1-O1		2.612	2.612
O2-O2		2.268	2.310
		2.424	2.413

Notes: The MD method and interatomic potential parameters are the same as those described in Murakami et al. (2004).

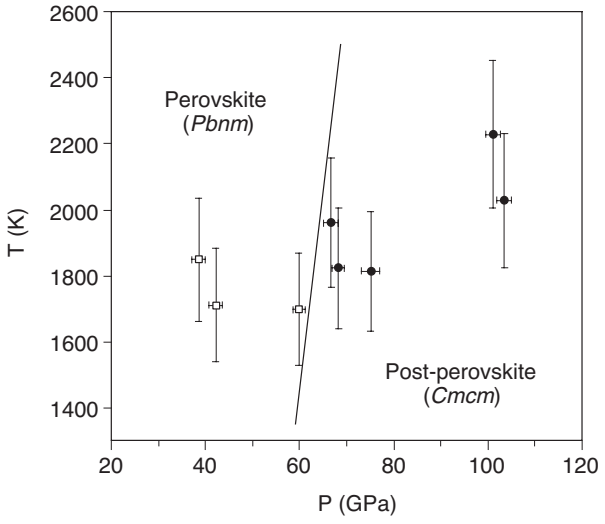

FIGURE 2. Phase diagram for $MgGeO_3$. Open squares and closed circles indicate the stabilities of perovskite and post-perovskite phase, respectively. The Clapeyron slope of the phase transition boundary is estimated to be +8 MPa/K.

TABLE 3. Lattice parameters and volumes of post-perovskite phase

P (GPa)	*a* (Å)	*b* (Å)	*c* (Å)	Volume (Å^3)
78.55 (21)	2.613 (0)	8.474 (1)	6.446 (1)	142.75 (3)
78.32 (12)	2.613 (0)	8.473 (1)	6.443 (1)	142.63 (3)
75.73 (30)	2.618 (0)	8.490 (1)	6.456 (1)	143.47 (3)
72.27 (15)	2.628 (0)	8.533 (1)	6.485 (1)	145.39 (4)
55.36 (17)	2.655 (1)	8.646 (4)	6.559 (3)	150.58 (11)
54.37 (23)	2.663 (2)	8.642 (6)	6.560 (3)	150.95 (18)
41.65 (32)	2.688 (2)	8.807 (11)	6.623 (8)	156.82 (31)
19.60 (56)	2.735 (2)	9.022 (6)	6.790 (6)	167.54 (23)
6.25 (34)	2.775 (6)	9.261 (14)	6.905 (13)	177.45 (60)

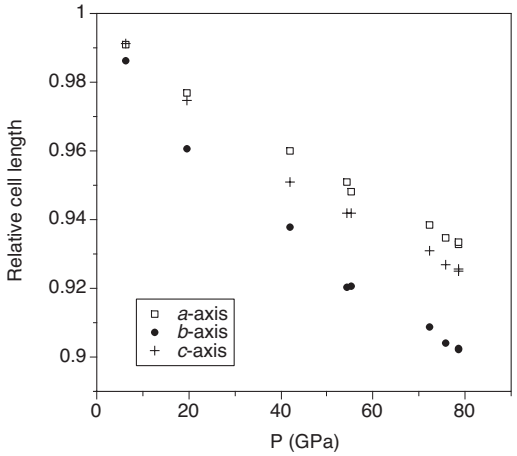

FIGURE 3. Relative cell length at 300 K as a function of pressure. Each unit-cell parameter was normalized to that at ambient condition (assumed: $a_0 = 2.800$, $b_0 = 9.390$, and $c_0 = 6.965$ Å).

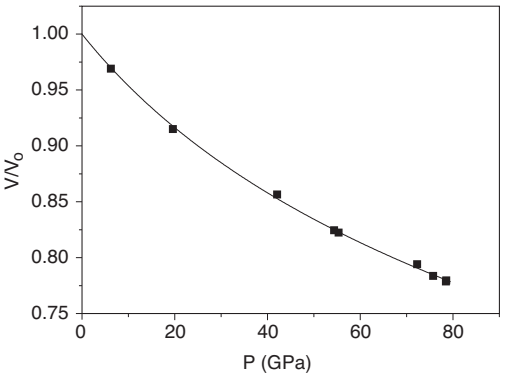

FIGURE 4. Pressure-volume data for $MgGeO_3$ post-perovskite phase fitted to the Birch-Murnaghan equation of state.

DISCUSSION

These results confirm that a $GdFeO_3$-type $MgGeO_3$ perovskite undergoes a pressure-induced phase transition to a $CaIrO_3$-type post-perovskite structure (space group *Cmcm*), in the same way as $MgSiO_3$ perovskite. The transition pressure of 63 GPa at 1800 K in $MgGeO_3$ is much lower than 125 GPa at 2500 K in $MgSiO_3$, which is consistent with the idea that germinates are the low-pressure analogues of silicates (Ross and Navrotsky 1988; Leinenweber et al. 1994).

Germanium is six-coordinated in both the perovskite and post-perovskite structures. Ono et al. (2003) demonstrated that α-PbO_2-type GeO_2 transforms to a pyrite (modified fluorite)-type phase above 80 GPa at 1500 K, with an increase in the coordination number of germanium from six to eight. Our present study shows that $MgGeO_3$ post-perovskite is stable to at least 103 GPa at 2030 K. With further increasing pressure, it possibly undergoes a structural phase transition to another $MgGeO_3$ polymorph with eightfold Ge coordination or decomposes into simple oxides.

In the post-perovskite phase, the SiO_6 (or GeO_6)-octahedra share edges to make an octahedral chain like that of rutile-type structures (Murakami et al. 2004). These chains run parallel to **a** and are interconnected by apical O atoms in the **c** direction to form edge- and apex-shared octahedral sheets. The octahedral sheets are stacked along **b**-axis with interlayer Mg^{2+} ions. Murakami et al. (2004) showed on the basis of MD calculations that the **b**-axis is more compressible than are the **a**- and **c**-axes in the $MgSiO_3$ post-perovskite phase. Our experiments consistently demonstrated a greater compressibility along **b** in the $MgGeO_3$ post-perovskite phase, which could be due to the stacked sheet structure along **b**. The post-perovskite phase has a strong elastic anisotropy.

ACKNOWLEDGMENTS

We thank Y. Tatsumi, H. Suematsu, and O. Shimomura for their support with the LHDAC experimental setup. J-F. Lin and an anonymous reviewer provided constructive comments. The in-situ X-ray measurements were conducted at SPring-8 (proposal no. 2003B2013LD2-np).

REFERENCES CITED

Ashida, T., Miyamoto, Y., and Kume, S. (1985) Heat capacity, compressibility, and thermal expansion coefficient of ilmenite-type $MgGeO_3$. Physics and Chemistry of Minerals, 12, 129–131.

Birch, F. (1947) Finite elastic strain of cubic crystals. Physical Review, 71, 809–924.

Hammersley, A.P. (1997) Fit-2d: in introduction and overview. European Synchrotron Radiation Facility Internal Report ESRF97HA02T.

Holmes, N.C., Moriarty, J.A., Gathers, G.R., and Nellis, W.J. (1989) The equation of state of platinum to 660 GPa (6.6 Mbar). Journal of Applied Physics, 66, 2962–2967.

Ito, E. and Matsui, Y. (1979) High-pressure transformations in silicates, germanates, and titanates with ABO_3 stoichiometry. Physics and Chemistry of Minerals, 4, 265–273.

Izumi, F. and Ikeda, T. (2000) A Rietveld-analysis program RIETAN-98 and its applications to zeolites. Materials Science Forum, 321–324, 198.

Kurashina, T., Hirose, K., Ono, S., Sata, N., and Ohishi, Y. (2004) Phase transition in Al-bearing $CaSiO_3$-rich perovskite: implications for seismic discontinuities in the lower mantle. Physics of the Earth and Planetary Interiors, 145, 67–74.

Leinenweber, K., Wang, Y., Yagi, T., and Yusa, H. (1994) An unquenchable perovskite phase of $MgGeO_3$ and comparison with $MgSiO_3$ perovskite. American Mineralogist, 79, 197–199.

Murakami, M., Hirose, K. Kawamura, K., Sata, N., and Ohishi, Y. (2004) Post-perovskite phase transition in $MgSiO_3$. Science, 8 April 2004 (10.1126/science.1095932).

Ono, S., Tsuchiya, T., Hirose, K., and Ohishi, Y. (2003) High-pressure form of pyrite-type germanium dioxide. Physical Review B, 68, 014103.

Ozima, M. and Akimoto, S. (1983) Flux growth of single crystals of $MgGeO_3$ polymorphs (orthopyroxene, clinopyroxene, and ilmenite) and their phase relations and crystal structures. American Mineralogist, 68, 1199–1205.

Ross, N.L. and Navrotsky, A. (1988) Study of the $MgGeO_3$ polymorphs (orthopyroxene, clinopyroxene, and ilmenite structures) by calorimetry, spectroscopy, and phase equilibria. American Mineralogist, 73, 1355–1365.

Sato, Y., Ito, E., and Akimoto, S. (1977) Hydrostatic compression of ilmenite phase of $ZnSiO_3$ and $MgGeO_3$. Physics and Chemistry of Minerals, 2, 171–176.

Saxena, S.K., Dubrovinsky, L.S., Lazor, P., Cerenius, Y., Hagkvist, P., Hanfland, M., and Hu, J. (1996) Stability of perovskite ($MgSiO_3$) in the earth's mantle. Science, 274, 1357–1359.

Shim, S.H., Duffy, T.S., and Shen, G. (2001) Stability and structure of $MgSiO_3$ perovskite to 2300-kilometer depth in earth's mantle. Science, 293, 2437–2440.

Watanuki, T. Shimomura, O. Yagi, T., Kondo, T., and Isshiki, M. (2001) Construction of laser-heated diamond anvil cell system for in situ X-ray diffraction study at SPring-8. Review of Scientific Instruments, 72, 1289–1292.

MANUSCRIPT RECEIVED MAY 8, 2004
MANUSCRIPT ACCEPTED SEPTEMBER 1, 2004
MANUSCRIPT HANDLED BY YINGWEI FEI